Surface & Coatings Technology 206 (2012) 2602–2615

Contents lists available at SciVerse ScienceDirect

Surface & Coatings Technology

journal homepage: www.elsevier.com/locate/surfcoat

Theoretical and experimental study on laser surface hardening by repetitive laser pulses

Ashish Kumar Nath *, Aniruddha Gupta, Frederick Benny

Department of Mechanical Engineering, Indian Institute of Technology Kharagpur, Khargapur-721302, India

ARTICLE INFO

Article history:
Received 13 July 2011
Accepted in revised form 12 November 2011
Available online 20 November 2011

Keywords:
Laser
Surface hardness
Repetitive pulses
Microhardness
Microstructure

ABSTRACT

An analytical solution for the temperature variation in a semi-infinite workpiece heated by repetitive laser pulses has been derived and the effects of various process parameters, viz. laser power, beam diameter, scan speed, pulse duration, repetition frequency and duty cycle on the surface transformation hardening have been investigated. The study shows that the soaking time of the top surface layer at a temperature above the phase transformation temperature, on which the homogeneity of microstructure and the depth of hardening depend, can be increased by repetitive laser pulse heating in comparison to continuous wave laser heating. The depth of hardness increases with the number of incident laser pulses at low frequencies in the range of Hz. This has been demonstrated by comparing the surface hardness characteristics of AISI 1055 steel specimens resulted by the continuous wave and repetitive laser pulse hardening processes.

1. Introduction

Laser surface hardening, first reported in the early seventies has become an established technology in manufacturing industry to enhance the surface characteristics in selected areas of various engineering components [1–3]. This has been revolutionizing automobile and aerospace industries for hardening surface layers of the turbine blades, crankshafts, piston ring grooves and tractor engine components, etc [4–9]. Laser hardening process gives a wear-resistant surface layer, thereby increasing the service life of components to a considerable extent. All cast iron, medium-carbon steel and tool steel are amenable to the laser hardening process [3,10–17]. The basic steps involved in laser transformation hardening of hypo-eutectoid steel consisting of pearlite (P) and pro-eutectoid ferrite (α), are the following:

(i) *Heating a surface layer by laser to a temperature above the phase transformation temperature Ac_1 of steel.* At this temperature the pearlite colonies begin to transfer to austenite, and the carbon from the newly formed high content austenite tends to diffuse in low-carbon content pro-eutectoid ferrite (α) at a rate determined by the temperature. A part of ferrite transforms to austenite (γ), depending upon the temperature with respect to the austenization temperature, Ac_3.

(ii) *Holding the surface layer above Ac_1 temperature for enough time for carbon diffusion and homogenization of austenite.* The carbon distribution becomes uniform in the microstructure of surface layer when it is kept above Ac_1 temperature for a sufficiently long time. When temperature exceeds Ac_3, ferrite gets transformed completely to austenite.

(iii) *Subsequent fast cooling for the transformation of austenite to martensite.*

A high power laser beam can be delivered to the workpiece with a very precise spatially and temporally control. For the localized laser heating, bulk of the workpiece remains at a low temperature and acts as a heat sink and therefore, when laser irradiation is stopped, rapid self-quenching takes place. The heating and cooling rates in 10^3–10^4 K/s range are typically realized in the laser hardening process. At such fast cooling rates laser irradiated surface layer becomes almost fully martensite, which enhances the surface wear and corrosion resistance and also the fatigue strength of workpiece [3].

Since the first demonstration of laser hardening process with a high power CO_2 laser, extensive theoretical modeling and experimental investigations have been carried out to develop a better understanding of the effects of various laser and process parameters on the surface characteristics, microstructure, residual stress, and surface hardening of various engineering components of different geometries and grades of steel [3,10–29].

Steen and Courtney established an empirical relation between the depth of hardening, z and the laser processing parameters, namely laser power, P, beam diameter, d, and laser scanning velocity, v [11]. A linear relationship between the hardening depth, z and a parameter, $P/\sqrt{(d.v)}$ was established that fitted well with the experimental results. Similar relationship was found by Lusquinos et al. in their investigation of laser surface hardening of AISI 1045 steel [17]. The main process parameters in their laser hardening experiment were

* Corresponding author. Tel.: +91 9932199975(mobile); fax +91 3222 255303.
E-mail address: aknath@mech.iitkgp.ernet.in (A.K. Nath).

0257-8972/$ – see front matter © 2011 Elsevier B.V. All rights reserved.
doi:10.1016/j.surfcoat.2011.11.019

tuned from the prediction realized by the numerical analysis of heat conduction involved in the process. Kou et al. carried out a theoretical and experimental study of the heat flow and laser phase transformation hardening of AISI 1018 steel [20]. They developed a three-dimensional heat flow model to obtain the temperature distribution during laser processing, which matched well with the prediction of the analytical solution of Carslaw and Jaeger [21]. They explained the microstructure of hardened zone with the help of the calculated peak temperature, heating and cooling rates. They observed a small amount of ferrite present in the hardened zone at the top surface, which they attributed to insufficient time allowed for the carbon to diffuse in austenite. Ashby and Easterling modeled the laser surface hardening process by combining an approximate solution for the temperature field with the equations describing the kinetics of structure changes [22]. They considered that the structural changes during heating were diffusion controlled and the extent of change would depend on the carbon diffusion coefficient and 'kinetic strength' of the heating cycle. They also considered that the austenite having carbon content greater than a critical value of 0.05 wt.% would transform to martensite on quenching at a fast rate, and the rest having carbon less than the critical value would revert to ferrite in medium carbon steel. They concluded that the most important parameters that controlled the hardening process were the laser energy density and beam interaction time, besides the composition and microstructure of steel. Davis et al. estimated the time above Ac_3 temperature that the workpiece must remain for carbon to diffuse and considered this in their model for the homogenization of austenite [23]. Ohmura et al. developed a finite-difference model to analyze the changes with time of heat flow, carbon redistribution in austenite and subsequent quenching to martensite during the laser hardening process [24]. Meijer and Sprang showed through their experimental and theoretical study that while the laser hardening process depended on two independent parameters, namely the absorbed laser power density and beam interaction time for a given depth of hardening, the maximum surface temperature was the only necessary control parameter to optimize the hardness and residual stress, etc. [25]. Jacot and Rappaz developed a two-dimensional diffusion model for the prediction of phase transformation and subsequently a combined model for describing the dissolution of pearlite, transformation of pro-eutectoid ferrite to austenite, homogenization and grain growth of austenite [26,27]. They found that the finishing temperature of austenitic transformation, Ac_3 depended on the carbon content and the heating rate. The Ac_3 temperature increased with the heating rate between two extreme values, 770 °C and 912 °C for medium carbon steel. They calculated the austenite homogenization temperature also, which increased from 800 °C to 1200 °C with the increase of heating rate from 0.1 K/s to 1000 K/s [26]. The calculated values compared well with the experimental results reported in the literature [26]. Na and Yang have also shown through their theoretical and experimental studies that the start of austenization temperature, Ac_1 and the finish of austenitic transformation temperature, Ac_3 increase with the heating rate in laser transformation hardening process [28]. Kommanduri and Hou presented a thermal analysis of the laser hardening process, which facilitated the prediction and optimization of the process parameters for practical applications [29]. The kinetic strength of heating cycle presented by Ashby and Easterling [22] and the variation of homogenization temperature with heating rate reported by Jacot and Rappaz [26] suggest that a finite soaking time above the phase transformation temperature is necessary to get a uniform distribution of carbon in austenite microstructure.

The lasers which have been commonly used for laser surface treatments, are high power CO_2 [1,2,11–13,18,19,21] and Nd:YAG Lasers [15,18,30–33]. In the last decade high power diode lasers with flat-top intensity profile have paved their way in these applications and are becoming very popular [16,34–36]. Some of the laser-hardening studies have been conduced with the diode pumped fiber laser also [17]. Lasers operating in both continuous wave (CW) [11–20,36] and pulsed modes [18,30–33] have been used. Danileiko et al. reported that the pulse-periodic laser beam was better suited to produce surface hardening compared to CW laser beam because of the additional process controlling parameters, viz. pulse duration and pulse frequency besides the laser intensity and scan speed, which could ensure better homogenization of austenitic phase, microhardness and hardening depth [30]. Experimental investigation was carried out with a quasi-cw Nd: YAG laser of 4 ms pulse duration operating at 50 Hz frequency. From their analysis of the thermal cycle in pulse-periodic laser heating they concluded that the carbon dissolution was cyclically cumulative and this increased the fraction of martensite in the irradiated region and the process efficiency.

Recent research efforts are directed towards the predictive modeling [37–40], simulation of multi-track laser hardening and tempering [41–43], and investigations of the effects of unconventional laser beam geometries and different temporal pulse shapes on the hardening process [44–47]. Miokovic et al. presented a detailed analysis of the effect of inhomogeneous austenitic formation, and heating and cooling rates on the resultant phase formation using a coupled heat conduction and phase transformation model [37]. Skvarenina and Shin presented a predictive modeling based on a three-dimensional thermal model coupled to a two-dimensional kinetic model for phase distribution and experimental results on laser hardening of AISI 1516 steel shafts with a complex feature [38]. Orazi et al. proposed a new austenization model for fast heating processes based an austenization time parameter to predict the hardness distribution along depth [39]. Shin and his co-workers have developed a predictive model for the residual stress induced in laser hardening and the tempering effect in multi-track processing [40,41]. Fortunato et al. [42] and Tani et al [43] have also developed a mathematical model for predicting the softening effects due to overlapping laser trajectories. Study of Safdar et al. presented the effect of laser beam geometry on transformation hardening [44]. Their study showed that the triangular shaped laser beam produced the best temperature history to achieve the highest hardness compared to the commonly used beams of circular and rectangular shapes. Leung et al. presented theoretical and experimental studies on laser hardening by customized beam [45]. They derived an exact solution solving a Klein-Gordon equation with expansion in Fourier series and integral combination for modeling the moving-interface heat transfer in the laser hardening process, and illustrated for a laser beam with a flat-top rectangular configuration.

In recent years, surface hardening with pulsed laser has attracted much research interest since this has wider scope for selective surface hardening with better process control than CW laser [31–33,46,47]. Habedank et al., with their experimental and simulation study, established that the pulse laser hardening with low-pulse frequencies (25–100 Hz) enabled a higher hardening depth compared to that by CW laser, and could generate compressive residual stresses leading to higher endurance limits [31]. Mahmoudi et al. studied the effect of peak and average laser powers, laser pulse width and overlapping of spots and tracks on the surface hardness of AISI 420 stainless steel with a pulsed Nd:YAG laser at 15 Hz frequency and found that the laser peak laser was a more important parameter than the average power [32]. Jiang et al. found that laser pulse energy was the main significant parameter affecting the depth and diameter of the spot hardened by a single Nd:YAG laser pulse in AISI 01 tool steel [33]. They also suggested using laser pulse durations much greater than 8 ms for achieving higher hardening effects. Wu et al. have developed a three-dimensional model for the pulsed laser transformation hardening considering the spatial and temporal laser intensity distribution and their results indicated that the temporal pulse shape had great effects on the hardening parameters [46]. Miokovic et al. have reported increase in hardening depth with the increase of number of laser pulses in the spot hardening process of AISI 4140 workpiece [47].

They carried out laser hardening experiments at the heating rates of 1000 and 10000 K/s and the cooling rates of 1000 and 3000 K/s for up to 27 cycles. The temperature history for the cyclic laser heating and cooling has been studied numerically as well as analytically by several researches [30,48–50]. Danileiko et al. calculated the thermal cycle of pulse-periodic laser interaction by solving the one-dimension heat conduction equation with boundary condition corresponding to irradiating the surface by a series of rectangular laser pulses of equal intensity [30]. Smurove et al. have analyzed the heating, melting, evaporation and solidification including velocity and position of phase boundaries by numerical modeling [48]. Kalyon and Yilbas derived a close form solution for the temperature during heating and cooling cycles using a Laplace transformation method and presented results for two laser pulses [49]. Yilbas and coworkers have investigated the laser consecutive pulse heating of solid surface and the influence of laser pulse parameters on the melting and mushy zone formation in the irradiated region by numerical simulation [50]. From various studies presented in the above papers [31–33,46,47] it is seen that the pulse periodic laser hardening has been investigated at frequencies ranging between 0.25 Hz and 100 Hz. However, the effect of laser repetition frequency and duty cycle has not been systematically investigated.

In this paper, analytical solutions of the one-dimensional heat conduction equation for temperature variation during the heating and cooling cycles in repetitive laser pulse (RLP) irradiation have been presented, and the effects of pulse on-time, pulse off-time, number of laser pulses, beam diameter and laser peak power on the temperature distribution and depth of hardening have been studied. Investigation was done in a wide frequency range starting from 1 Hz to 1000 Hz. It is seen that the average heating rate reduces and the soaking time, for which a surface layer is maintained above the phase transformation temperature, increases significantly in case of RLP heating compared to CW heating for a constant laser power density. This can facilitate homogenization of austenite and increase in depth of hardening. Experimental study was carried out on AISI 1055 steel specimens with a 2 kW fiber laser in CW and repetitive pulse modes. The surface temperature (time) profiles were monitored at different RLP irradiating frequency and compared with the calculated results. The microhardness measurement and scanning electron microscopic observation revealed that the depth of hardening and the homogeneity of microstructure was more in case of RLP heating than those with CW laser. In spot hardening, the depth of hardening increased with the number of laser pulses incident at a low repetition frequency.

2. Analytical modeling

Temperature profile: For the thermal analysis, it has been assumed that heat is transferred to the specimen by a source providing a constant heat flux, specimen is semi-infinite and heat conduction is one dimension. For these assumptions to be valid, the thermal diffusion length should be much smaller than the physical dimensions of workpiece and the laser beam diameter at the surface. The temperature change in the material as a function of time, t and depth, z can be given by the 1-D heat conduction equation [21]

$$\frac{\partial^2 T(z,t)}{\partial z^2} = \frac{1}{\alpha}\frac{\partial T(z,t)}{\partial t} \tag{1}$$

where α is the thermal diffusivity of the workpiece material.

For a constant extended heat source incident on a semi-infinite workpiece, an analytical solution of Eq. (1) for the temperature rise can be given by [21].

$$\Delta T(z,t) = 2\frac{I}{k}\sqrt{\alpha t}\ \ ierfc\left(\frac{z}{2\sqrt{\alpha t}}\right) \tag{2}$$

where I is the absorbed laser power density at the surface and k is the thermal conductivity of workpiece material.

During the cooling cycle after the end of laser pulse or dwell time, t_p the temperature rise for $t > t_p$ can be given by [21]

$$\Delta T(z,t) = 2\frac{I}{k}\left[\sqrt{\alpha t}\ \ ierfc\left(\frac{z}{2\sqrt{\alpha t}}\right) - \sqrt{\alpha\left(t-t_p\right)}\,ierfc\left(\frac{z}{2\sqrt{\alpha\left(t-t_p\right)}}\right)\right]. \tag{3}$$

In case of a CW laser scanned over the surface at a velocity v, the dwell time, t_p at any point on the surface is given $t_p = \mathrm{d}/\mathrm{v}$, where d is the laser beam diameter.

The above solutions hold good for a beam diameter greater than the thermal diffusion length which is given by 2 $(\alpha t_p)^{1/2}$. If the beam diameter is comparable to thermal diffusion length, the heat loss along the radial direction is not negligible. Taking the radial heat loss into account, temperature variations during the heating and cooling cycles can be given by the following equations:

Temperature rise during heating cycle [2,21]:

$$\Delta T(z,t) = 2\frac{I}{k}\sqrt{\alpha t}\left[ierfc\left(\frac{z}{2\sqrt{\alpha t}}\right) - ierfc\left(\frac{\sqrt{z^2+a^2}}{2\sqrt{\alpha t}}\right)\right]. \tag{4}$$

Temperature variation during cooling cycle, $t > t_p$:

$$\Delta T(z,t) = 2\frac{I}{k}\left[\sqrt{\alpha t}\left\{ierfc\left(\frac{z}{2\sqrt{\alpha t}}\right) - ierfc\left(\frac{\sqrt{z^2+a^2}}{2\sqrt{\alpha t}}\right)\right\} - \sqrt{\alpha\left(t-t_p\right)}\left\{ierfc\left(\frac{z}{2\sqrt{\alpha\left(t-t_p\right)}}\right) - ierfc\left(\frac{\sqrt{z^2+a^2}}{2\sqrt{\alpha\left(t-t_p\right)}}\right)\right\}\right] \tag{5}$$

Here 'a' is the laser beam radius.

In case of the multiple pulses incident on workpiece, the final temperature can be determined by taking into account the heating and cooling cycles of all previous laser pulses. Thus, for the temperature rise during the 2nd laser pulse, Eq. (4) can be extended as the following:

$$\begin{aligned}\Delta T(z,t) = 2\frac{I}{k}\sqrt{\alpha}\Bigg[&\sqrt{t}\left\{ierfc\left(\frac{z}{2\sqrt{\alpha t}}\right) - ierfc\left(\frac{\sqrt{z^2+a^2}}{2\sqrt{\alpha t}}\right)\right\}\\ &-\sqrt{\left(t-t_p\right)}\left\{ierfc\left(\frac{z}{2\sqrt{\alpha\left(t-t_p\right)}}\right) - ierfc\left(\frac{\sqrt{z^2+a^2}}{2\sqrt{\alpha\left(t-t_p\right)}}\right)\right\}\\ &+\sqrt{t-\left(t_p+t_c\right)}\left\{ierfc\left(\frac{z}{2\sqrt{\alpha\left(t-\left(t_p+t_c\right)\right)}}\right)\right.\\ &\left.-ierfc\left(\frac{\sqrt{z^2+a^2}}{2\sqrt{\alpha\left(t-\left(t_p+t_c\right)\right)}}\right)\right\}\Bigg].\end{aligned} \tag{6}$$

Here t_p and t_c are the laser pulse on-time and off-time respectively. The first four '*ierfc*' terms account for the heating and cooling cycles of the first laser pulse and the last two terms are for the heating cycle of the 2nd laser pulse.

Generalizing the Eq. (6) for 'n' number of laser pulses the temperature rise during the $(n+1)$th laser pulse can be given by Eq. (7).

$$\Delta T(z,t)_{heating} = 2\frac{I}{k}\sqrt{\alpha}\left[\sum_{n=1}^{n}\left\{\sqrt{t-(n-1)\left(t_p+t_c\right)}\left(ierfc\left(\frac{z}{2\sqrt{\alpha\left(t-(n-1)\left(t_p+t_c\right)\right)}}\right)-ierfc\left(\frac{\sqrt{z^2+a^2}}{2\sqrt{\alpha\left(t-(n-1)\left(t_p+t_c\right)\right)}}\right)\right)-\sqrt{t-\left(nt_p+(n-1)t_c\right)}\left(ierfc\left(\frac{z}{2\sqrt{\alpha\left(t-\left(nt_p+(n-1)t_c\right)\right)}}\right)-ierfc\left(\frac{\sqrt{z^2+a^2}}{2\sqrt{\alpha\left(t-\left(nt_p+(n-1)t_c\right)\right)}}\right)\right)\right\}+\sqrt{t-n\left(t_p+t_c\right)}\left(ierfc\left(\frac{z}{2\sqrt{\alpha\left(t-n\left(t_p+t_c\right)\right)}}\right)-ierfc\left(\frac{\sqrt{z^2+a^2}}{2\sqrt{\alpha\left(t-n\left(t_p+t_c\right)\right)}}\right)\right)\right]. \quad (7)$$

Similarly, the temperature during the cooling cycle after the $(n+1)$ th laser pulse can be given by Eq. (8),

$$\Delta T(z,t)_{cooing} = 2\frac{I}{k}\sqrt{\alpha}\left[\sum_{n=1}^{n}\left\{\sqrt{t-n\left(t_p+t_c\right)}\left(ierfc\left(\frac{z}{2\sqrt{\alpha\left(t-n\left(t_p+t_c\right)\right)}}\right)-ierfc\left(\frac{\sqrt{z^2+a^2}}{2\sqrt{\alpha\left(t-n\left(t_p+t_c\right)\right)}}\right)\right)-\sqrt{t-\left((n+1)t_p+nt_c\right)}\left(ierfc\left(\frac{z}{2\sqrt{\alpha\left(t-\left((n+1)t_p+nt_c\right)\right)}}\right)-ierfc\left(\frac{\sqrt{z^2+a^2}}{2\sqrt{\alpha\left(t-\left((n+1)t_p+nt_c\right)\right)}}\right)\right)\right\}\right]. \quad (8)$$

Eqs. (7) and (8) were solved using MATLAB 7.6.0 and the absorbed laser power density, I and interaction time, t_p were estimated to heat an AISI 1055 steel specimen up to a depth of 0.5 mm to a temperature above AC_3 temperature without melting the surface. As Meijer et al. [25] and Jacot and Rappaz [27] have suggested that the surface layer should be heated about 50 °C above the AC_3 temperature for homogenization of austenite, therefore surface layer temperature above1230 K was taken in the calculation for predicting the depth of hardening.

The composition and thermo-physical properties of AISI 1055 steel considered for the calculations are as the following [51]:

Composition : C = 0.5−0.6%, Mn = 0.6−0.9%, P = 0.04%,
S = 0.04%, Si = 0.15−0.3%, Fe = balance.

Thermo-physical properties: Thermal conductivity, k = 51.9 W/m.K; density, ρ = 7865 kg/m^3; specific heat, C_p = 472 J/kg-K; melting temperature = 1765 K and phase transformation temperature, Ac_1 = 996 K, Ac_3 = 1183 K.

The absorbed laser power density and interaction time required to raise the surface layer temperature up to 0.5 mm depth above 1230 K without surface melting were estimated to be 5750 W/cm^2 and 510 ms respectively. Fig. 1 shows the calculated temperature distribution at the surface and 0.5 mm depth for the absorbed CW laser power density of 5750 W/cm^2. From Fig. 1 it is seen that the soaking time of layer at 0.5 mm depth is about 400 ms.

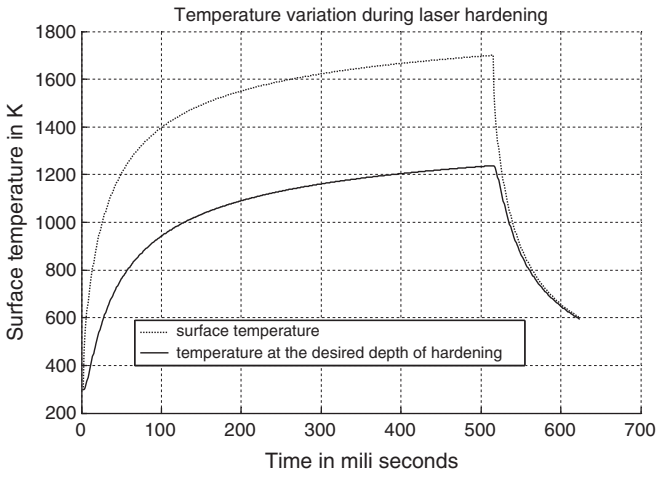

Fig. 1. Calculated temperature profiles at the surface and 0.5 mm depth for absorbed laser power density = 5750 W/cm^2 and laser irradiation time = 510 ms.

The depth of hardening and soaking time can be increased by reducing the laser power density and correspondingly increasing the interaction time as reported by Meijer et al. [25]. Fig. 2 shows the effect of laser power density on the maximum depth up to which temperature is above 1230 K and the laser interaction time for surface to reach a maximum temperature without the onset of melting, for two different laser beam diameters. The soaking time can be approximated with the laser interaction time for the fast heating rates (>10^3 K/s), typical of the laser hardening process, as seen in Fig. 1. Fig. 2a and b is for 1700 K and 1600 K surface temperature respectively and the numbers in parentheses are the laser interaction time. As can be seen in Fig. 2, the depth of hardening is more at lower laser power densities, corresponding to which interaction time is longer. With the increase of laser power density surface reaches to the maximum temperature sooner, and

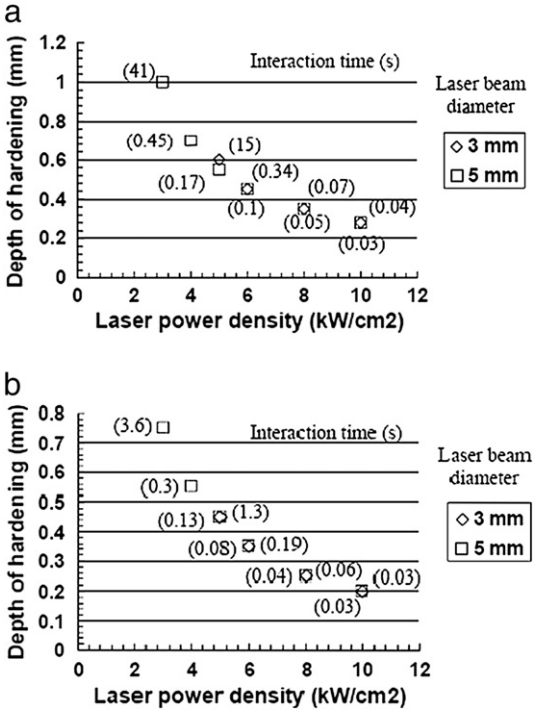

Fig. 2. Variation of the maximum predicted depth of hardening with laser power density for two laser beam diameters; numbers in parentheses are interaction time; maximum surface temperature: (a) 1700 K (b) 1600 K.

therefore the laser interaction time and the depth up to which hardening could be feasible are reduced. Comparison of the hardening depth for two different laser beam diameters shows that a higher hardening depth can be achieved with a larger diameter beam at a relatively lower laser power density. Another observation is that the depth of hardening is same for both laser beam diameters at a constant laser power density, but the laser interaction time is much longer in case of the smaller diameter beam than that for the larger diameter beam, and the difference is more significant at lower laser power densities. For example, at 10^4 W/cm^2 power density surface reaches to 1700 K temperature in 38 ms and 32 ms with 3 mm and 5 mm diameter beam respectively, and at 5×10^3 W/cm^2 power density corresponding time durations are 15 s and 170 ms respectively. This is because of the relatively less heat conduction loss in radial direction in case of the larger diameter beam. The upper limit of surface temperature also influences the depth of hardening. Comparison of Fig. 2a and b shows that the hardening depth and interaction time are reduced when the surface temperature is lowered from 1700 K to 1600 K.

The effect of repetitive laser pulse heating on temperature distribution was studied at low (~1 Hz) and high (~100 Hz) laser pulse frequency ranges. Fig. 3a–c show the temperature distribution at the surface and 0.5 mm depth for the peak laser power density of 5750 W/cm^2 at 1, 2, 3 Hz frequencies and 50% duty cycle. It is seen that the average heating rate is significantly reduced and the soaking time is increased with the increase of pulse repetition frequency. Though the peak and average powers are constant in these three cases, more number of laser pulses is needed at a higher repetition frequency than that at a lower frequency to raise the surface temperature to a constant value. This is because of the lower rise in temperature for individual shorter duration laser pulse and the more frequent cooling in between two consecutive laser pulses at a higher frequency. The dependence of soaking time on duty cycle (30%–60%) at 5750 W/cm^2 laser power density and 1 Hz repetition frequency is shown in Fig. 4. The laser interaction time and correspondingly the soaking time are increased with the reduction of duty cycle because of the increased cooling time between two laser pulses and the reduced average laser power.

At high repetition frequencies (≥100 Hz) the absorbed laser power density of 5750 W/cm^{2}could not raise the surface temperature near melting point even in 50 s of laser interaction time. Therefore, calculations for high frequencies were carried out at a higher laser power density of 10 kW/cm^2. For comparison, temperature profiles at the surface and a depth where temperature rise is about 1230 K are shown for 10, 20, 50 and 100 Hz frequencies in Fig. 5a–d respectively. At this laser power density the depth up to which temperature is raised to 1230 K is ~0.28 mm. The general trend of variation is similar to that of the low pulse repetition frequency, i.e. the number of laser pulse needed to heat surface layer up to a set temperature and soaking time increases, and the heating rate decreases with the increase of repetition frequency. One significant difference in repetitive pulse heating at low and high frequency ranges is that the surface layer cools down to a temperature below the starting temperature of martensite formation, $T_{ms}=670$ K, during each cooling cycle at lower frequencies (<10 Hz), Fig. 3; but at frequencies above 20 Hz, there is not enough time during the cooling cycle for the surface layer to cool down below this temperature, Fig. 5. If the laser power density is lowered the number of laser pulses required for heating the surface to a set temperature, the soaking time and the hardening depth, all are increased, and temperature comes down below T_{ms} during only a few initial cooling cycles, as shown in Fig. 5e for 8000 W/cm^2 power density at 20 Hz repetition frequency. And, when the duty cycle is reduced the effects are similar to that of lowering the laser power density, however in this case the increase in the hardening depth is less, and the number of cooling cycles during which temperature comes down below T_{ms} is increased. This can be seen in

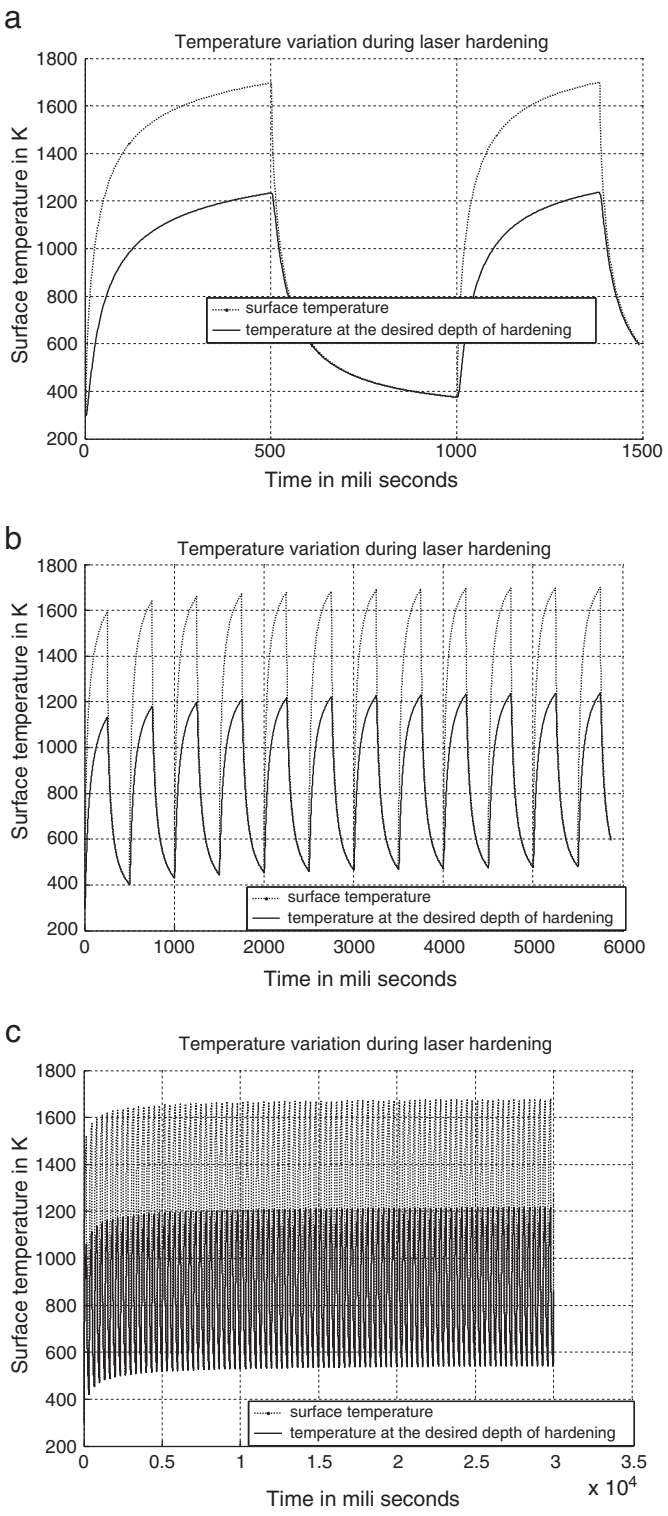

Fig. 3. Calculated temperature distribution at the surface and 0.5 mm depth at different laser pulse frequencies (a)1 Hz (b) 2 Hz (c) 3 Hz; duty cycle = 50%, peak laser power density = 5750 W/cm^2.

Fig. 5f which shows the temperature distribution at 10^4 W/cm^2 power density and 20 Hz repetition frequency with duty cycle reduced to 33.6%. For fair comparison the number of laser pulses and the interaction time in both cases (Fig. 5e and f) are kept same.

Microhardness profile: In hypo-eutectoid plain carbon steel as the temperature increases above Ac_1 value during heating cycle, the pearlite colonies, first transforms to austenite and the carbon from

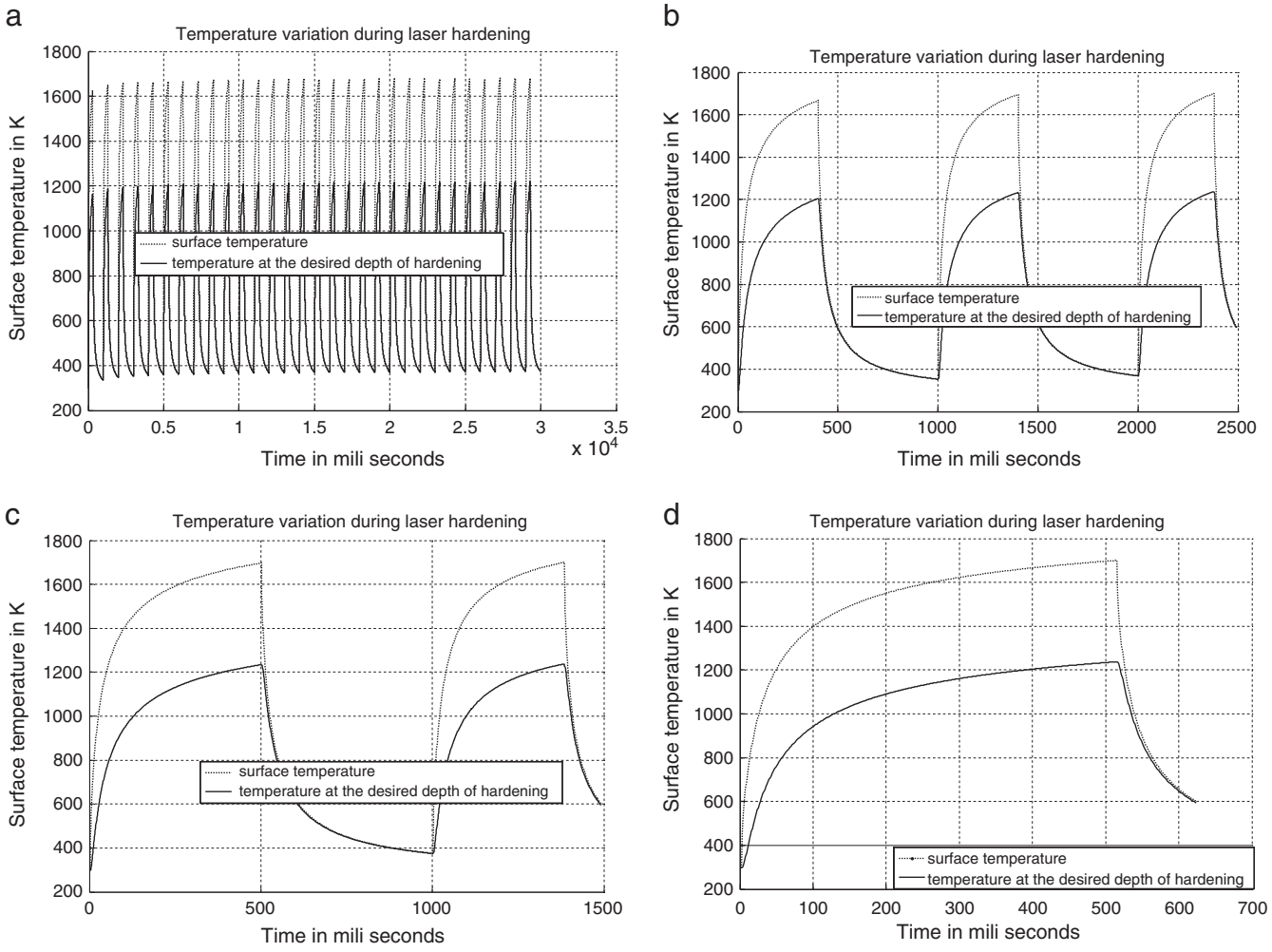

Fig. 4. Calculated temperature distribution and soaking time duration, t_s for different duty cycles (DC) at 5750 W/cm^2 laser power density and 1 Hz repetition frequency, (a) DC = 30% DC, t_s ~ 10 s (b) DC = 40%, t_s ~ 1 s (c) DC = 50% DC, t_s ~ 0.66 s (d) DC = 60%, t_s ~ 0.4 s.

the eutectoid cementite plates diffuses into eutectoid ferrite plates present in pearlite colonies. In this process pearlite becomes austenite containing 0.8 wt.% carbon. Depending upon the temperature with respect to Ac_3 temperature, a part of proeutectoid ferrite also is transformed into austenite with negligible carbon content. Carbon diffuses from the high carbon content austenite colonies to the low carbon content proeutectoid ferrite and austenite colonies to an extent which is determined by the temperature and the time duration for which the surface layer is held above Ac_1 temperature. During heating cycle, as the surface layer reaches to Ac_3 temperature, transformation of proeutectoid ferrite to austenite is complete. The diffusion rate of carbon is higher in ferrite than in austenite and it increases with temperature [22]. Depending upon the temperature above Ac_1, a finite time is required for the carbon dissolution in pearlite colonies and some addition time for the homogenization of complete austenite phase by carbon diffusion from high to low concentration regions [22,26].

The time required for carbon to diffuse in pearlite structures can be estimated by Eq. (9) [22]

$$Ll = 2D_0\alpha\ \tau\ \exp(-Q/RT_p) \tag{9}$$

where 2L is the diameter of the pearlite colony, λ is the average pearlite plates spacing, and D_0, Q, R, and T_p respectively are the pre-exponential carbon diffusivity, activation energy for transformation, gas constant, and peak temperature. 'τ' can be called as a characteristic time for the diffusion of carbon in pearlite. The constant α can be approximated as [22]

$$a \approx 3(RT_p/Q)^{1/2}. \tag{10}$$

The diameter of pearlite colony can be related to the austenite grain diameter, g as the following [22]:

$$2L = g/f_i^{1/3}. \tag{11}$$

Here, $f_i = C/C_e$, C = carbon wt.% of the steel specimen and $C_e \approx 0.8$ wt.% in the eutectoid steel.

Fig. 6 shows a SEM micrograph of the as-received AISI 1055 steel specimen. From the micrographs of different zones the average values of pearlite colony diameter, 2L ≈ 30 μm and ferrite plates spacing, λ = 0.5 μm are estimated. The time duration for carbon diffusion in pearlite for these values is estimated using Eq. (9) at different temperatures in Ac_1–Ac_3 interval and is tabulated at sr. no. 1 in Table 1. Values of D_0, Q and other material properties are taken from literature [22]. From the estimated time it is apparent that the diffusion of carbon in pearlite at temperatures above Ac_1 temperature is very fast, and during heating the surface layer to Ac_3 temperature at a heating rate as high as 10^4 K/s, transformation of pearlite to austenite can be assumed to be almost instantaneous.

Diffusion of carbon from austenite having carbon content C_e = 0.8 wt.% into pro-eutectoid ferrite and austenite is govern by

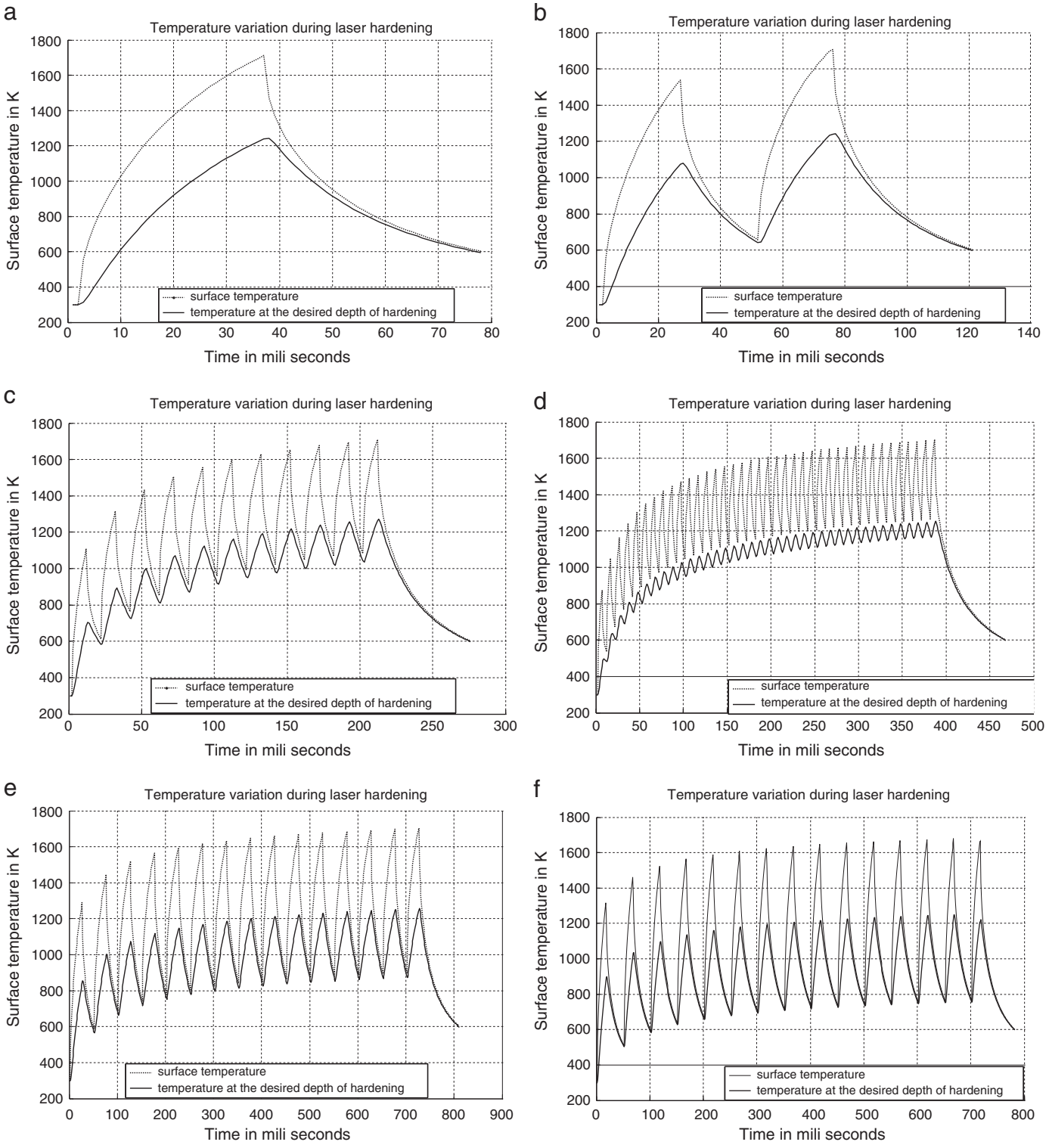

Fig. 5. Calculated temperature profiles at the surface and a depth, d up to which temperature is ~1230 K, for repetitive laser pulse heating at different frequencies, f, laser power density, $I = 10^4$ kW/cm^2, duty cycle (DC) = 50% (a) f = 10 Hz, d = 0.28 mm (b) f = 20 Hz, d = 0.28 mm (c) f = 50 Hz, d = 0.28 mm (d) f = 100 Hz; d = 0.3 mm (e) $I = 8 \times 10^3$ W/cm^2, f = 20 Hz, DC = 50%, d = 0.36 mm (f) I = 10 kW/cm^2, f = 20 Hz, DC = 33.6%, d = 0.3 mm.

the Fick's 2nd law and the characteristic time for carbon diffusion in pro-eutectoid ferrite, $\tau_{p-\alpha}$ and austenite, $\tau_{p-\gamma}$ can be estimated using an approximate solution given by Eq. (12) [22].

$$x = (2/\sqrt{\pi})\left(D_0 \alpha \tau \exp - \left(Q/RT_p\right)\right)^{1/2} \ln(C_e/2C_c) \quad (12)$$

Here, x is the distance up to which carbon content in pro-eutectoid ferrite/austenite reaches a critical value, C_c by diffusion from high carbon content (C_e = 0.8wt.%) austenite in time, τ. The critical value, C_c is taken as 0.05 wt.% for martensite to form [22,26]. For the homogenization of austenite, carbon should diffuse in the whole austenite grain. Equating x with the radius of austenite grain

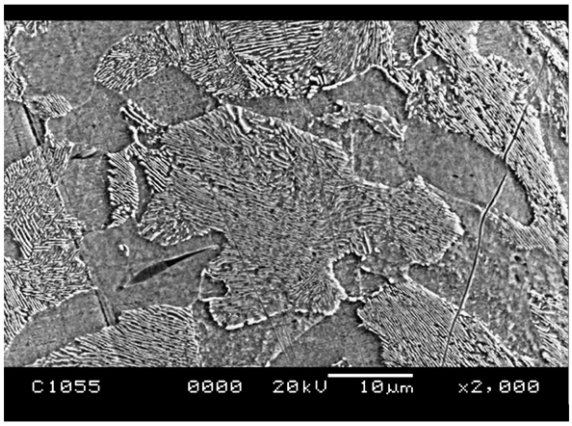

Fig. 6. SEM micrograph of as-received AISI 1055 steel specimen.

(g/2), values of $\tau_{p-\alpha}$ and $\tau_{p-\gamma}$ were estimated for different temperatures above Ac_1 and are tabulated at sr. no. 2 and 3 respectively in Table 1. Diffusion of carbon is relatively very slow in austenite than in ferrite, therefore much longer soaking time, of the order of a few seconds is needed for the complete homogenization of austenite, if the surface layer is heated above Ac_1 temperature at a very fast rate ($\geq 10^4$ K/s).

After heating the surface layer above Ac_3 temperature when this is cooled below martensite transformation temperature, T_{ms} at a fast rate ($\geq 10^3$ K/s), austenite having carbon more than critical value C_c transforms to martensite and the rest to ferrite or retained austenite. The volume fraction of martensite in the surface layer heated above Ac_3 temperature and then quenched, can be estimated by Eq. (13) [22]

$$f = f_m - (f_m - f_i)\exp - \left[6 f_i^{2/3} x/g\right]. \quad (13)$$

Here, f_m is the maximum volume fraction of martensite permitted by the phase diagram,

$$f_m = \begin{cases} f_m = 0 & \text{if } T_p < Ac_1 \\ f_i + (1-f_i)\left\{\left(T_p - Ac_1\right)/(Ac_3 - Ac_1)\right\} & \text{if } Ac_1 < T_p < Ac_3 \\ f_m = 1 & \text{if } T_p > Ac_3 \end{cases}.$$

With the knowledge of the martensite volume fraction, average microhardness of martensite/ferrite mixture in the quenched surface layer can be estimated by Eq. (14), which has been reported to predict the microhardness in agreement with the experimental results in medium carbon ($0.1 < c < 0.8$) steel [22]

$$H(VHN) = 1667C - 926\, C^2/f + 150. \quad (14)$$

The volume fraction, f of martensite in AISI 1055 steel with 0.5 wt.% carbon heated above Ac_3 temperature estimated by putting $x = g/2$ in Eq. (13) is nearly 1. Average microhardness, corresponding to $f = 1$, is estimated to be 752 VHN. In the region where peak temperature is in between Ac_1 and Ac_3, martensite volume fraction and microhardness will be less. The microhardness distribution is expected to be non-uniform, since the carbon content in martensite will be varying in 0.05–0.8 wt.% range.

In repetitive pulse heating at a low frequency (~1 Hz), the surface layer temperature will undergo cyclic variation as shown in Fig. 3a–c, and the diffusion of carbon during each pulse will push forward the boundary having critical value of carbon, C_c. Therefore, the depth of hardness is expected to increase with the number of incident laser pulse at low frequencies. This has been schematically shown in Fig. 7. The depth is expected to saturate with the increase in number of laser pulses, since the gradient of carbon content will reduce after irradiation by each laser pulse. At high frequencies and CW heating the onset of surface melting will limit the interaction time and the depth of hardening.

3. Experimental results and discussion

Experimental study was carried out on as-received AISI 1055 steel specimens using a 2 kW fiber laser (YLR 2000) integrated with an optical beam delivery system and a five-axes CNC workstation to investigate the effects of CW and repetitive pulse heating on surface hardening. This can be operated in CW and modulated modes. The modulation frequency and duty cycle can be varied in 1–1000 Hz and 5–100% ranges respectively. A 10 mm diameter collimated laser beam of M^2 parameter ~15 comes out of the optical fiber beam delivery system. The laser beam was focussed with a 200 mm focal length lens and the workpiece was kept beyond the focal point where the defocused laser beam diameter was 3 mm at the workpiece surface. Throughout the laser hardening experiments 3 mm diameter beam was used. Specimens of two different sizes, $30 \times 12 \times 10$ mms and $12 \times 10 \times 1.2$ mms dimensions were used. Surfaces to be laser treated, were polished with emery (220grade) paper, cleaned and coated with the black permanent marker to increase the surface absorptivity. The absorptivity of the polished and coated surfaces was estimated by measuring the incident and reflected laser powers from the surface with a laser power meter (model-COMET-10K-V1 ROHS OPHIR make, accuracy ±5%). The power meter needs a continuous laser exposure of 10 s for each measurement. Measurements were done at different incident laser powers and it was observed that the coating was getting tarnished within the 10 s laser exposure. The average value of absorptivity was estimated to be ~43% for the bare polished surface and in 60–70% range with coating. The relatively large variation in absorptivity in case of coated surface was possibly due to the variation in the coating thickness and uniformity in different sets of measurement.

In order to confirm that the surface temperature could follow the fast variation of high frequency repetitive laser pulse heating, surface temperature was measured with the help of a non-contact infrared (IR) sensor (Micro-Epsilon make, model no. CTLM-2HCF3-C3H, temperature range = 385 °C to 1600 °C, response time = 1 ms) during the heating process of a workpiece. The surface temperature profiles during repetitive laser pulse heating at 100 Hz frequency with 20% and 50% duty cycles are shown in Fig. 8a and b respectively. The estimated absorbed laser power density was 10 kW/cm^2. For comparison, the temperature profile calculated for the same cyclic laser heating conditions of 50% duty cycle using room temperature thermal properties is also shown in Fig. 8c. From Fig. 8a it can be seen that the surface temperature could follow the 2 ms duration heating cycles

Table 1
Characteristic time for carbon diffusion in pearlite and austenite at different temperatures.

Sr. no.	Peak temperature→	1000 K	1113 K	1183 K	1273 K	1473 K	1673 K
1.	Characteristic time, τ_{p-a} for carbon diffusion in Pearlite	1.1 ms	0.4 ms	0.23 ms	–	–	–
2.	Characteristic time, $\tau_{p-\alpha}$ for carbon diffusion from Pearlite (transformed to austenite) to Pro-eutectoid Ferrite	10 ms	3.2 ms	2.0 ms			
3.	Characteristic time, $\tau_{p-\gamma}$ for carbon diffusion from Pearlite (transformed to austenite) to Austenite	–	10 s	4 s	1.5 s	0.25 s	0.06 s

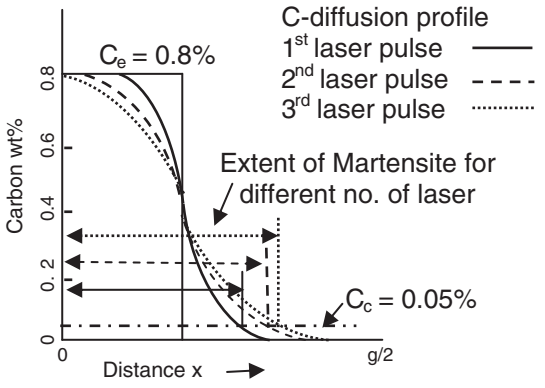

Fig. 7. Schematic of carbon diffusion for a number of laser pulses incident on the surface.

corresponding to100 Hz and 20% duty cycle. Faster cyclic variation in the surface temperature could not be detected reproducibly due to the limitation of 1 ms response time of the IR sensor. Because of the uncertainty in the emissivity of coated surface, which depends on the wavelength of emitted radiation, temperature and measuring arrangement, comparison of the measured and calculated absolute peak temperatures was not attempted. Instead, the depth of temperature modulation during the cyclic heating, defined as $(T_{max}-T_{min})/T_{max}$ were compared. Here T_{max} and T_{min} are the maximum and minimum surface temperature during one heating and cooling cycle. The depth of temperature modulation will depend mainly on the thermal properties of the workpiece. The experimental and calculated depth of temperature modulations in Fig. 8b and c are about 24% and 26% respectively. Kou et al. had reported that the temperatures calculated for cold rolled 1018 steel using variable thermal properties and high temperature thermal properties were in close agreement and the predictions based on the room temperature thermal properties were relatively on the higher side [20]. In the present study the results were in contrary. The temperature profiles calculated using high temperature (≥1073 K) thermal properties (specific heat = 624 J/kg K and thermal conductivity = 24.7 W/m K) [52] is shown in Fig. 8d. Calculation with high temperature thermal properties shows that the surface temperature crosses the melting temperature within 100 ms and reaches to about 2750 K in 400 ms duration of cyclic heating. But in actual experimental with the same cyclic laser heating conditions, whose temperature profile shown in Fig. 8b, no melting was observed. The depth of temperature modulation in this case is about 19%, more deviated from the experimental value in the lower side. Prediction of the relatively high rise in temperature and a lower depth of temperature modulation could be because of the lower

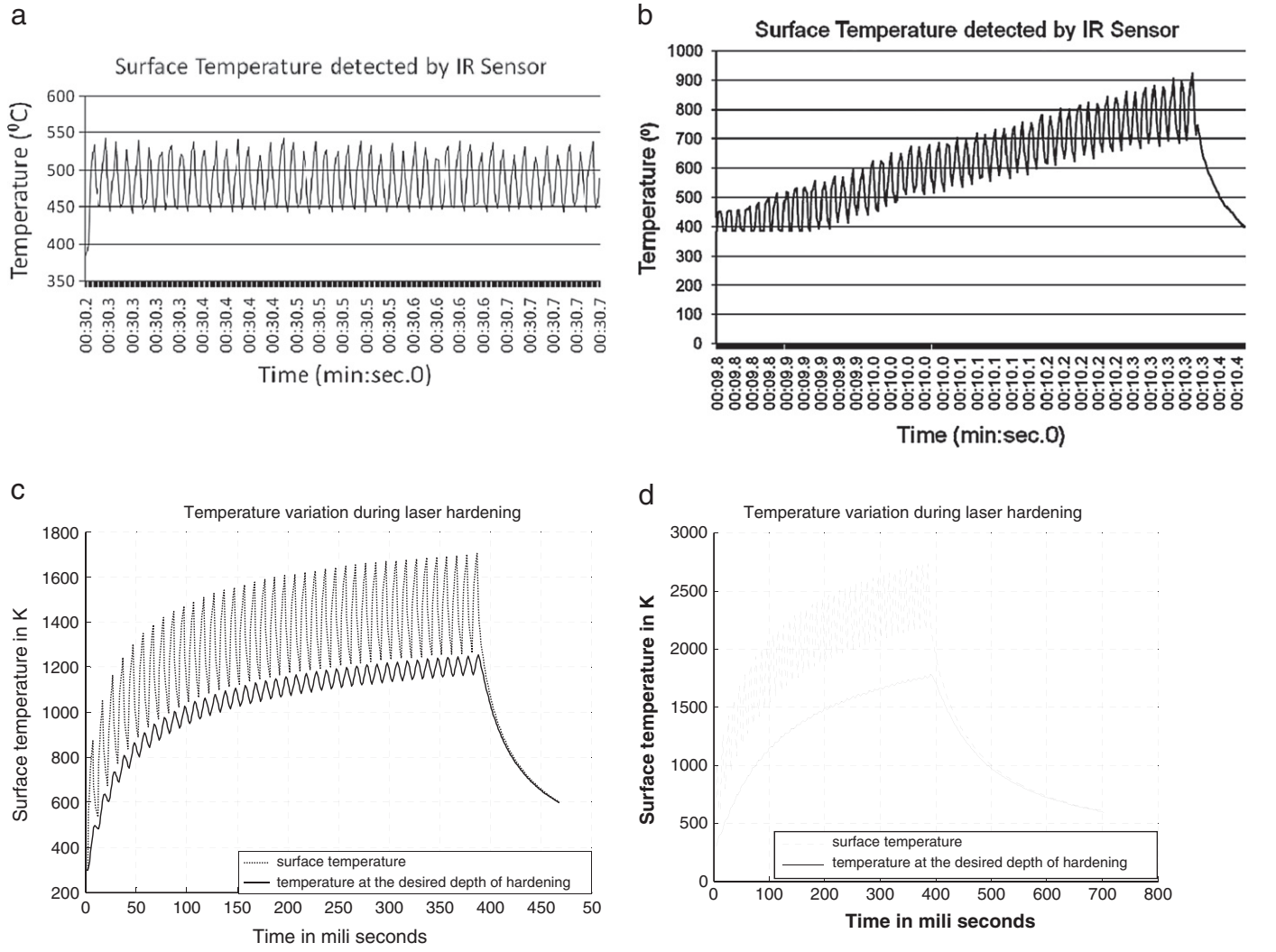

Fig. 8. Surface temperature monitored by a non-contact IR temperature sensor for different laser repetition frequencies and duty cycles (DC), laser intensity = 10 kW/cm^2, laser beam diameter = 3 mm (a) 100 Hz, DC = 20% (b) 100 Hz, DC = 50%; Calculated temperature profile 100 Hz, DC = 50% (c) using room temperature thermal properties (d) using high temperature thermal properties.

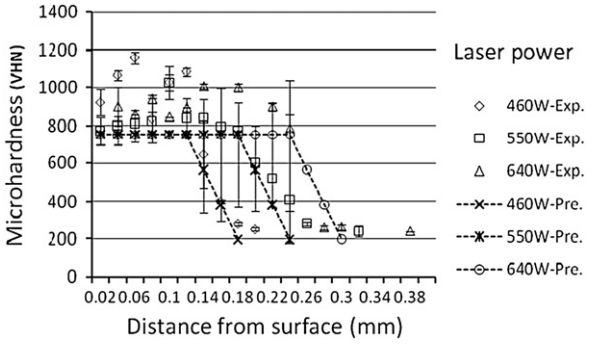

Fig. 9. Measured microhardness profiles at different CW laser powers, laser scan speed = 18 mm/s and comparison with predicted profiles.

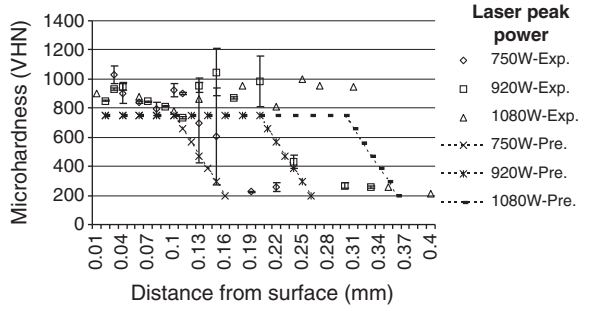

Fig. 10. Measured microhardness profiles for different peak laser powers, repetition frequency = 100 Hz, duty cycle = 50%, scan speed = 12 mm/s and comparison with predicted profiles.

value of the high temperature thermal conductivity of steel compared to that at room temperature. The difference of the present results from that that reported by Kou et al. [20] could be because of the difference in the temperature history in these two cases. Since the surface temperature modulation profile agreed closely to the calculated profile based on the room temperature thermal properties, therefore these were taken for all calculations in the present investigation.

For investigating the effects of laser pulse repetition frequency and duty cycle on the microhardness and depth of hardness, experimental ranges of laser power and scan speed were determined where there was no surface melting. For comparison between CW and RLP hardness, $P/\sqrt{(vd)}$ parameter on which depth of hardness depends was kept nearly constant [11,17,29].

Experiments with CW laser beam and RLP at 100–1000 Hz frequencies and 30–50% duty cycles were done on 10 mm thick specimens. After the laser treatment specimens were diamond polished and etched with nital solution. The microhardness measurements were done with 50 gf load for 15 s test duration. Measurements on some of the samples were done with 100 gf load also and the microhardness values, similar to those with 50 gf, were obtained. Figs. 9 and 10 respectively show the Vickers microhardness along the depth for CW and RLP hardening at different laser powers. The variations in microhardness in different measurements are also indicated in the figures. The depth up to which surface layer is heated above Ac_3 temperature and the soaking time duration were calculated using Eqs. (7) and (8), and the average hardness values were calculated using Eq. (14). Results of the theoretical calculations and experimental measurements are tabulated in Table 2. As one would expect, the peak surface temperature and the depth of hardness increased with the increase of laser power at a constant laser interaction time. Comparison between experimental and calculated values of hardening depth at a relatively low laser power (sr. no. 1 and 4 in Table 2) shows that they are in agreement for a temperature rise in the range of 1113–1183 K, while for a higher laser power (sr. no. 3 and 6 in Table 2) they match for a surface layer temperature of about 1230 K. Agreement at a higher temperature for the higher laser power could be because of the increase in the homogenization temperature with increased heating rate, as reported by Jacot and Rappaz [26]. Calculated heating rates are also tabulated in Table 2, which shows that the rate increased with the laser power, and is higher for CW heating than that for RLP heating, though the peak surface temperature is lower in the former case. The calculated microhardness profiles considering surface absorptivity in 60–70% range are also plotted in Fig. 9 and 10 along with the experimental results. The minimum microhardness is considered at a depth where temperature rise is just below Ac_1 temperature. Comparison of microhardness results of CW and RLP heating indicates that the depth of hardness depends on the soaking time duration as well as $P/\sqrt{(vd)}$ parameter. Maximum depth of hardness is achieved at the highest values of soaking time and $P/\sqrt{(vd)}$ in case of the RLP hardening (sr. no. 6 in Table 2). Further, since the heating rate is higher in CW case than that in RLP case, Ac_3 and homogenization temperatures will be higher in CW case. Under these experimental conditions the homogenization of austenite will be less in case of CW laser hardening compared to that in RLP hardening. The agreement between the experimental and calculated depths of hardening is reasonably good considering that the room temperature thermal properties have been taken in calculations.

The soaking time durations in all the above cases are longer than τ_{p-a} and $\tau_{p-\alpha}$, the characteristic time for carbon diffusion in pearlite and pro-eutectoid ferrite colonies respectively, but less than $\tau_{p-\gamma}$, the characteristic time of carbon diffusion in austenite, (Table 1). This would suggest that carbon from the high carbon content austenite could diffuse mainly to pro-eutectoid ferrite and very little to pro-eutectoid ferrite transformed austenite in the Ac_1–Ac_3 temperature range, except at the top surface layer where temperature is much higher than the Ac_3 temperature. The austenite phase will be more homogenized and the grain size will be larger at the top surface compared to that at depths where temperature rise is in the Ac_1–Ac_3 temperature range.

Table 2
Experimental and calculated depth of hardening for different laser processing conditions.

Sr. no.	Laser power (W)	Laser interaction time (ms)	Peak surface temperature (K)	Heating rates 10^3 K/s	Depth (mm) up to which temperature (T) is more than AC_3 temperature/Soaking time (s) (Prediction)			Experiment depth of hardness (mm)	$P/\sqrt{d.v}$ W/mm$\sqrt{s}$
					T = 1113 K	T = 1183 K	T = 1230 K		
CW laser hardness									
1	460	167	1260	7.5	0.16/88	0.08/108	0.04/116	0.14	62.5
2	550	167	1350	8.1	0.28/88	0.2/102	0.16/114	0.21	75.5
3	640	167	1470	8.8	0.36/92	0.3/100	0.24/116	0.25	87.0
Repetitive laser pulse hardness (100 Hz, 50% duty cycle)									
4	750	250	1300	5.2	0.14/72	0.1/90	0.06/100	0.12	62.5
5	920	250	1520	6.1	0.32/100	0.26/136	0.2/160	0.23	78.0
6	1080	250	1695	6.8	0.43/125	0.37/150	0.32/170	0.32	90.0

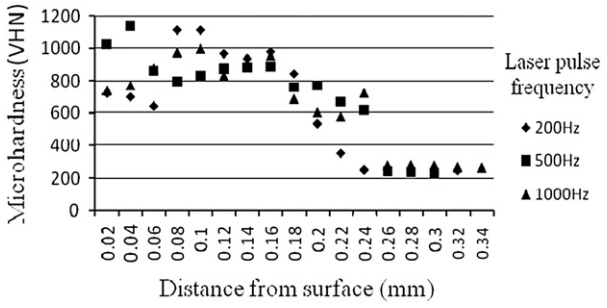

Fig. 11. Measured microhardness profiles at different repetition frequencies, Laser power = 1080 W, duty cycle = 30%, scan speed = 12 mm/s.

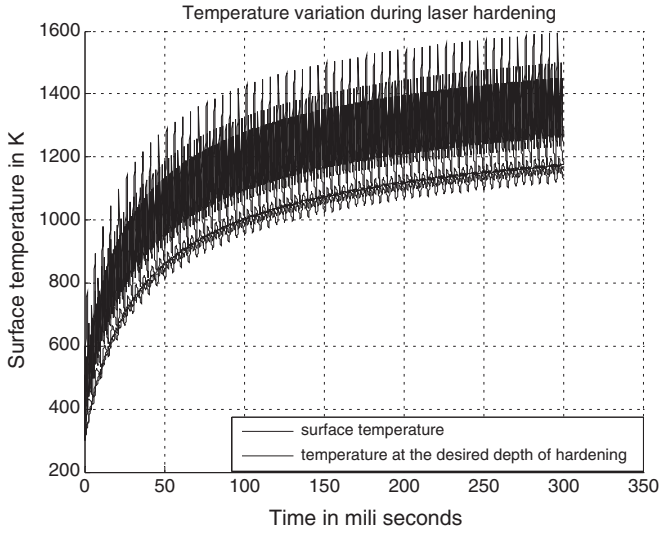

Fig. 12. Superimposed temperature profiles calculated at the surface and 0.22 mm depth for 200 Hz, 500 Hz and 1000 Hz repetition frequencies, laser power = 1080 W, beam interaction time = 300 ms.

The variation of microhardness profile with frequency in 200 Hz–1000 Hz range is shown in Fig. 11. This shows that there is not much difference in the depth of hardness with the change of frequency in this range. Calculated temperature profiles for different laser pulse frequencies are superimposed in Fig. 12. This shows that the average temperature rise is almost same in this frequency range and surface layer up to 0.22 mm depth is heated above 1150 K in all cases, resulting in a constant depth of hardening, similar to the experimental results presented in Fig. 11. To study the effect of duty cycle, surface hardening was carried out at 30% and 50% duty cycle. Microhardness profiles are presented in Fig. 13 which shows that the depth of hardness reduces with the reduction of duty cycle. This is because the

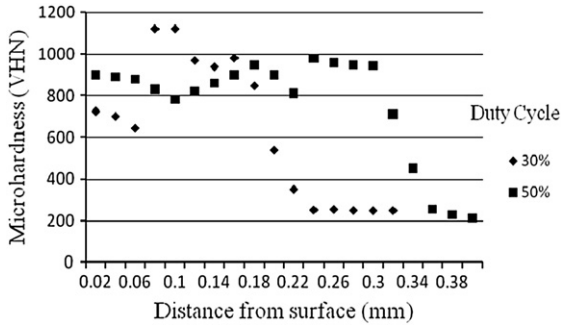

Fig. 13. Measured microhardness profiles for 30% and 50% duty cycles, laser power = 1080 W, frequency = 200 Hz, scan speed = 12 mm/s.

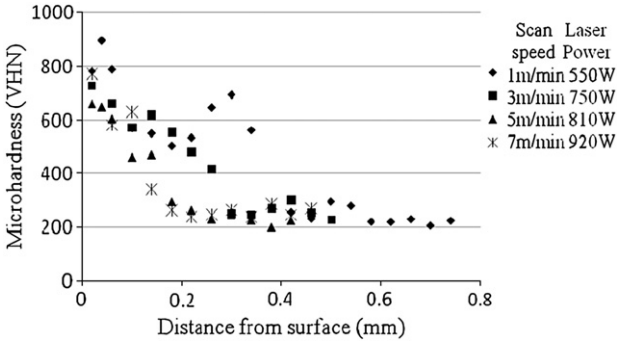

Fig. 14. Measured microhardness profiles fordifferent laser scan speeds at an optimum laser power for each scan speed without onset of surface melting.

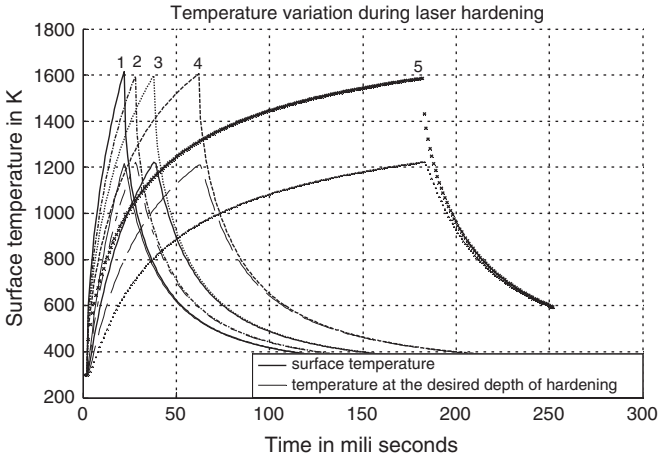

Fig. 15. Calculated temperature profiles for different scan speeds at the surface and depths up to which temperature reached to 1200 K; laser power and depths are given in Table 3; temperature profiles identified by 1, 2–5 correspond to 1,3, 5,7 and 9 m/min scan speed respectively.

average laser power decreases and the heat loss during laser off-period increases with the reduction of duty cycle.

The influence of laser scanning speed on CW laser hardening and the number of laser pulses incident at a stationary location at low frequencies (~1 Hz) were studied on 1.2 mm thick specimen. Fig.14 shows the microhardness profiles at different CW laser scan speeds. Laser power was optimized for each laser scan speed to maximize the depth of hardness without the onset of surface melting. Depth of hardness decreased with the increase of laser scan speed. Calculated temperature profiles for different scan speeds are plotted in Fig. 15, and values of the experimental parameters and the predicted and measured depth of hardness are tabulated in Table 3. This is found to vary nearly proportional to $P/\sqrt{(d.v)}$ parameter whose values are also tabulated in Table 3.

The optical macrographs of the transverse cross-section of laser hardened zone and the hardness profiles for different numbers of laser pulses of on-time, $t_{on} = 200$ ms and off-time, $t_{off} = 400$ ms are

Table 3
Experimental and calculated depth of hardening at different laser scan speeds and maximum laser power limited by the onset of surface melting.

Sr. no.	Laser scan speed (m/min)	Laser power (W)	Experimental depth (mm)	Predicted depth (mm)	$P/\sqrt{d.v}$ (W/mm$\sqrt{s}$)
1	1	600	0.38	0.36	85.9
2	3	775	0.28	0.30	63.3
3	5	910	0.24	0.24	57.6
4	7	1030	0.2	0.21	55.1
5	9	1165	0.18	0.20	54.9

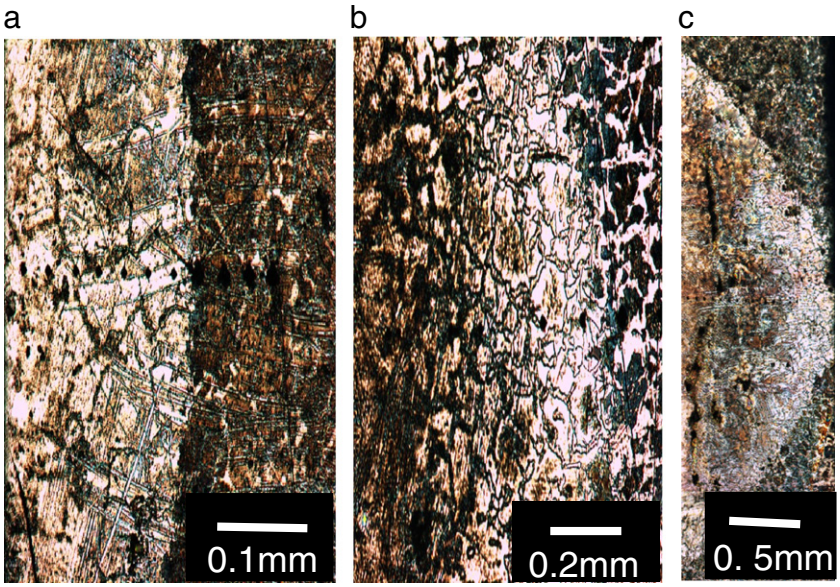

Fig. 16. Optical macrographs of laser surface hardened zone, laser power = 550 W, t_{on} = 200 ms, t_{off} = 400 ms (a) single laser pulse (b) 3 laser pulses and (c) 5 laser pulses.

presented in Fig. 16 and Fig. 17 respectively. Depth of hardness increased significantly with the number of laser pulses. Similar results were reported by Miokovic et al. for heating cycle of approximately 0.5–2.5 Hz frequencies [47]. The calculated hardening depths were 0.38, 0.44 and 0.46 mm for 1, 3 and 5 laser pulses respectively against the measured hardening depths of 0.36, 0.5 and 0.8 mm. The higher value of experimental depth of hardening than the calculated value, especially for multiple laser pulses could be because of the overall heating of the relatively thin specimen. The 1.2 mm specimen thickness is much smaller than the thermal diffusion length, $2\sqrt{\kappa\tau}$ for 200 ms laser pulse duration, therefore the prediction based on semi-infinite size specimen is expected to underestimate the depth of hardness.

Fig. 18 shows the hardness profiles produced by 3 laser pulses with different values of pulse off-time, t_{off}. Depth of hardness is

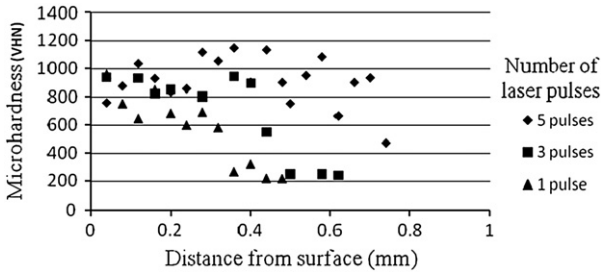

Fig. 17. Measured microhardness profiles for different number of laser pulses, laser power = 550 W, t_{on} = 200 ms, t_{off} = 400 ms.

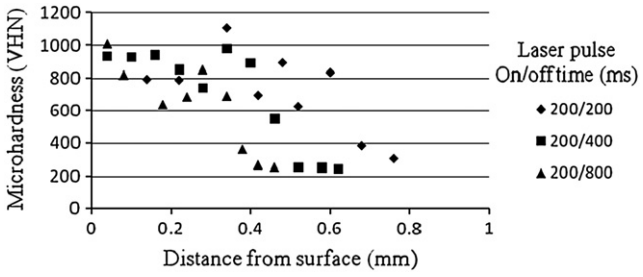

Fig. 18. Measured microhardness profile for different laser pulse off-times, laser power = 550 W, t_{on} = 200 ms, number of laser pulses = 3.

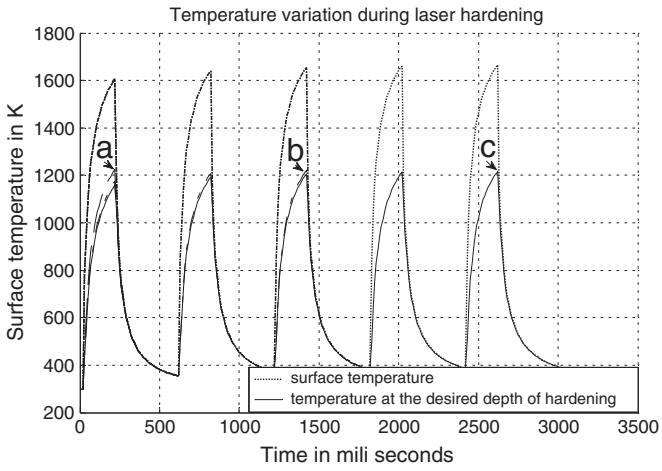

Fig. 19. Calculated temperature profiles for varying number of laser pulses, n, and predicted depth of hardening, d; laser power density = 6000 W/cm^2, t_{on} = 200 ms, t_{off} = 400 ms; (a) n = 1, d = 0.38 mm (b) n = 3, d = 0.44 mm (c) n = 5, d = 0.46 mm.

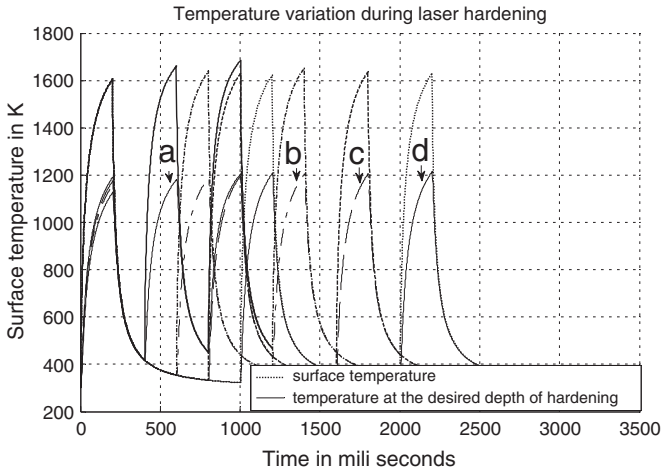

Fig. 20. Calculated temperature profiles for different t_{off} times, and predicted depth of hardening, d; laser power density = 6000 W/cm^2, t_{on} = 200 ms, (a) t_{off} = 200, d = 0.48 mm, (b) t_{off} = 400, d = 0.44 mm, (c) t_{off} = 600, d = 0.42 mm (d) t_{off} = 800 ms, d = 0.40 mm.

more when pulse off-time is shorter, as subsequent pulses after the first pulse see elevated surface temperatures. Corresponding to the measured hardening depths of 0.76 mm, 0.52 mm and 0.42 mm for three different values of $t_{off,}$ the calculated depths are 0.48 mm, 0.44 mm and 0.4 mm respectively. In this case also the experimental values are higher than the calculated values for shorter t_{off}, possibly because of the same reason as explained above. Figs. 19 and 20 show the calculated temperature profiles at the surface and depths where the temperature rise is about 1200 K for different numbers of laser pulse and different values of pulse off-time respectively.

The scanning electron microscope (SEM) images of the resulting microstructure were recorded at various points in the transverse section of the laser hardened region. Fig. 21(a–c) shows SEM images of

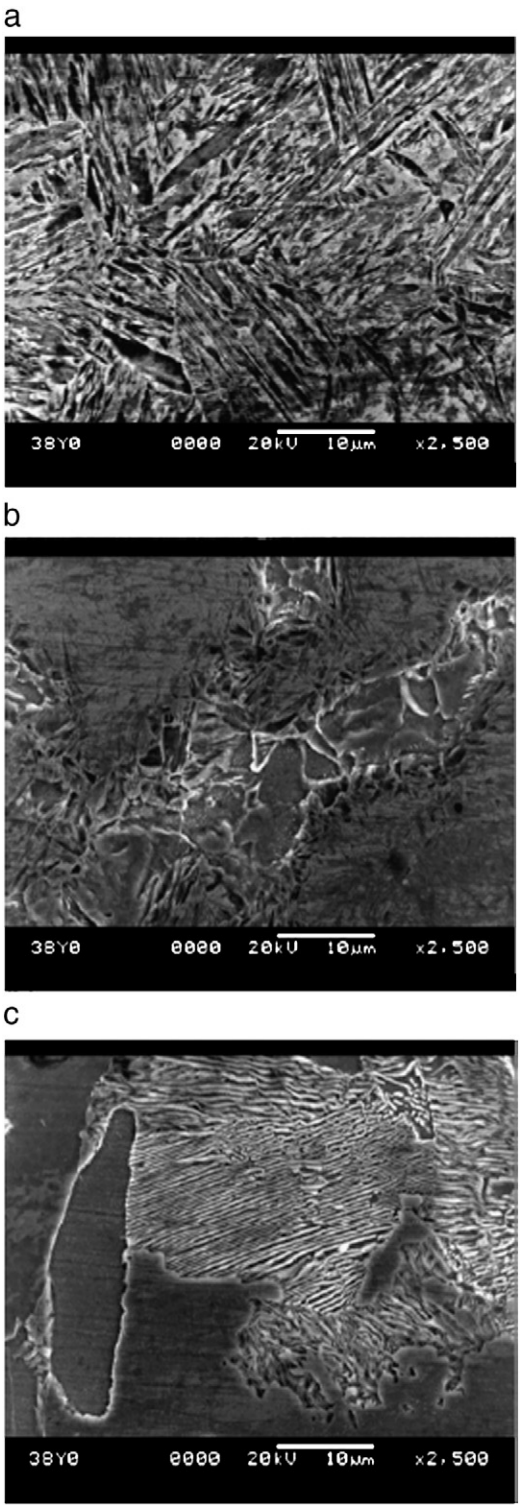

Fig. 21. SEM micrographs of laser surface hardened cross-section for CW laser irradiation, laser power = 640 W, laser scan speed = 18 mm/s (a) near the top surface (b) middle of the hardened region (c) near the boundary of HAZ and base material.

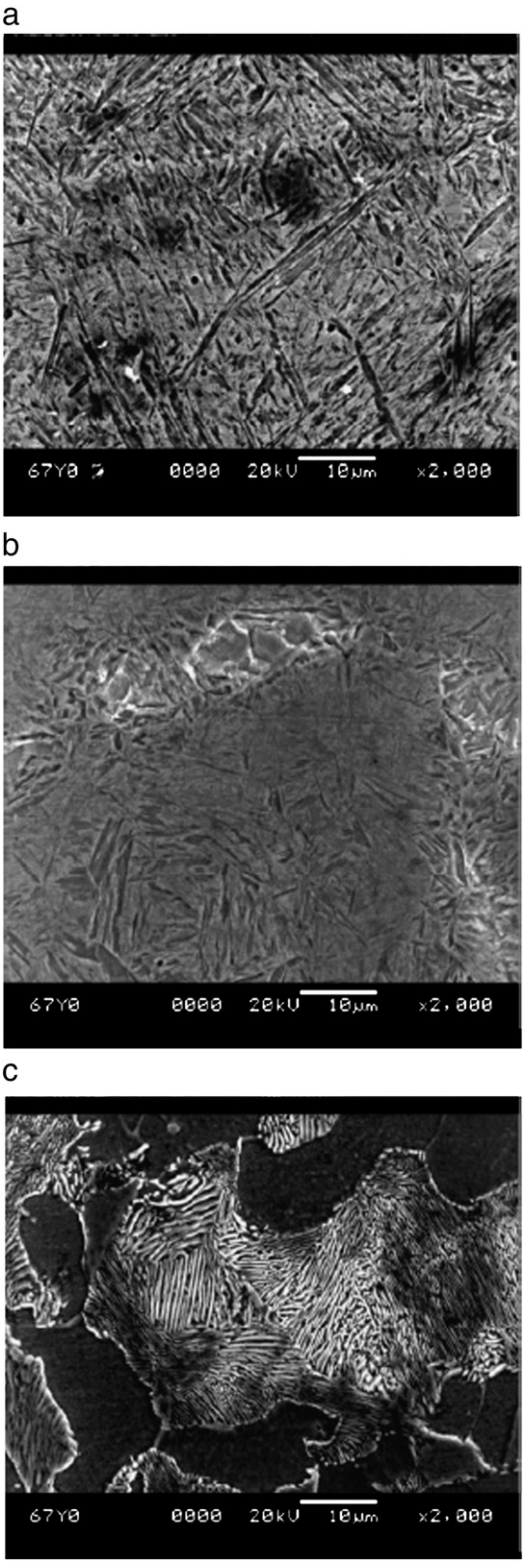

Fig. 22. SEM micrographs of laser surface hardened cross-section for repetitive pulsed laser irradiation, laser peak power = 1080 W, laser scan speed = 12 mm/s, pulse frequency = 100 Hz, duty cycle = 50% (a) near the top surface (b) in the middle of the hardened region (c) near the boundary of HAZ and base material.

different zones along the depth for CW laser hardening. The SEM micrograph of near top surface shows the formation of homogeneous martensite structure, Fig. 21a. However, the microstructure at the middle of the hardened zone shows the formation of heterogeneous martensite structure along with ferrite. This could be because of the relatively lower temperature rise of the middle region compared to that of the top surface, resulting in incomplete homogenization of austenite, Fig. 21b. The microstructure at the boundary of HAZ shows the lamellar pearlite in a ferrite (dark) field, Fig. 21c. Fig. 22(a–c) shows SEM images of the RLP hardening at 100 Hz frequency. Microstructures in Fig. 22a and b show that the homogeneous martensite laths have resulted along the depth. Comparison of Figs. 21b and 22b shows that RLP hardening could produce more uniform martensite structure than CW laser hardening. The microstructure at the boundary of HAZ in Fig. 22c is similar to that in Fig. 21c. The longer soaking time, slower heating rate and higher rise of temperature in RLP hardening compared to those in CW laser hardening (sr. no. 6 Table 2) could be the reasons for the more uniform martensite microstructure in the repetitive pulse hardening process.

4. Conclusions

In conclusion, analytical solutions for the temperature profiles of heating and cooling cycles in repetitive laser pulse irradiation have been derived and the effects of various process parameters such as laser power, beam diameter, scan speed, pulse duration, repetition frequency and duty cycle on the laser surface hardening have been investigated. In RLP hardening process the average heating rate was found to be lower and the soaking time above the phase transformation temperature longer than those in CW laser hardening process. These effects could increase the depth of hardness and facilitate better homogenization of the austenite phase. The depth of hardness increased with the number of laser pulses at low repetition frequencies and also with the reduction of inter-pulse time. The calculated and measured temperature profiles of the repetitive laser pulse heating and the depth of hardening were in good agreement in the specimen of dimensions larger than the thermal diffusion length.

Acknowledgement

The financial support for the high power Yb-fiber laser from the Department of Science and Technology, New Delhi, under the FIST Program-2007 (No.: SR/FIST/ETII-031/2007) is gratefully acknowledged.

References

[1] E. Locke, R. Hella, IEEE/OSA Conference on Laser Engineering and Applications (Washington DC, May 30-June1, 1973) paper −5.9, 1973, p. 33.
[2] J.W. Hill, M.J. Lee, I.J. Spalding, Opt. Laser Technol. 12 (1974) 276.
[3] K. Sridhar, A.S. Khanna, in: Narendra B. Dahotre (Ed.), Surface Engineering Series, Lasers in Surface Engineering, Vol.-1, ASM International, 1998.
[4] D.M. Roessler, Mater. Manuf. Processes 4 (1989) 285.
[5] Anon, Diesel Gas Turbine Worldwide 18 (1986) 10.
[6] Y.I. Mulin, V.A. Sokolov, Sov. Ener. Technol 5 (1989) 44.
[7] A.P. Androsov, S.I. Aleksenko, M.V. Boyarkin, V.G. Kusidis, V.I. Petrov, Met. Sci. Heat Treat. 30 (1988) 67.
[8] V.V. Divinskii, L.A. Medvedovskaya, G.A. Rainin, A.V. Sviridov, Sov. Electr. Eng. 59 (1988) 42.
[9] A.A. Ablaev, E.M. Birger, V.V. Divinskii, S.G. Drozdov, L.A. Medvedovskaya, Met. Sci. Heat Treat. 31 (1989) 12.
[10] J.R. Bradley, S. Kim, Metall. Trans. A 19A (1988) 2013.
[11] W.M. Steen, C.H.G. Courtney, Met. Technol. 6 (1979) 456.
[12] J. Senthil Selvan, K. Subramanian, A.K. Nath, J. Mater. Process. Technol. 91 (1999) 29.
[13] M.J. Tobar, C. Álvarez, J.M. Amado, A. Ramil, E. Saavedra, A. Yáñez, Surf. Coat. Technol. 200 (2006) 6362.
[14] A. Basu, J. Chakraborty, S.M. Shariff, G. Padmanabham, S.V. Joshi, G. Sundararajan, J. Dutta Majumdar, I. Manna, Scr. Mater. 56 (2007) 887.
[15] H. Pantsar, J. Mater. Process. Technol. 189 (2007) 435.
[16] H.J. Shin, Y.T. Yoo, D.G. Ahn, K. Im, J. Mater. Process. Technol. 187–188 (2007) 467.
[17] F. Lusquinos, J.C. Conde, S. Bonss, A. Riveiro, F. Quintero, R. Comesana, J. Pou, Appl. Surf. Sci. 254 (2007) 948.
[18] G. Tani, A. Fortunato, A. Ascari, G. Campana, CIRP Ann. Manuf. Technol. 59 (2010) 207.
[19] C. Soriano, J. Leunda, J. Lambarri, V. García Navas, C. Sanz, Appl. Surf. Sci. 257 (2011) 7101.
[20] S. Kou, D.K. Sun, Y.P. Le, Metall. Trans. A 14A (1983) 643653.
[21] H.S. Carslaw, J.C. Jaeger, Conduction of Heat in Solids, 2nd ed. Oxford University Press, London, 1959.
[22] M.F. Ashby, K.E. Easterling, Acta Metall. 32 (1984) 1935.
[23] M. Davis, P. Kapadia, J. Dowden, W.M. Steen, C.H.G. Courtney, J. Phys. D: Appl. Phys. 19 (1986) 1981.
[24] E. Ohmura, K. Inoue, K. Haruta, JSME Int J. Ser. 1: Solid Mech. Strength Mater. 32 (1) (1989) 45.
[25] J. Meijer, I. van Sprang, Ann. CIRP 40 (1) (1991) 183.
[26] A. Jacot, M. Rapaz, Acta Mater. 45 (2) (1997) 575.
[27] A. Jacot, M. Rapaz, Acta Mater. 47 (5) (1999) 1645.
[28] S.J. Na, Y.S. Yang, Surf. Coat. Technol. 34 (1988) 319.
[29] R. Komanduri, Z.B. Hou, Int. J. Mech. Tools Manuf. 44 (2004) 991.
[30] Y.K. Danileoko, A.M. Prokhorov, A.I. Pchelintsev, A.V. Sidorin, Sov. J. Quant. Electron. 16 (12) (1986) 1611.
[31] G. Habedank, J. Woitschig, T. Seefeld, W. Juptner, F. Vollertsen, R. Baierl, H. Bonas, P. Mayr, R. Schroder, F. Jablonski, R. Kienzler, Mater. Sci. Eng. A 488 (2008) 358.
[32] B. Mahmoudi, M.J. Torkamany, A.R. Sabour Rouh Aghdam, J. Sabbaghzade, Mater. Des. 31 (2010) 2553.
[33] J. Jiang, L. Xue, S. Wang, Surf. Coat. Technol. 205 (2011) 5156.
[34] L. Li, Opt. Lasers Eng. 34 (2000) 231.
[35] F. Bachmann, Appl. Surf. Sci. 208–209 (2003) 125.
[36] I.R. Pashby, S. Barnes, B.G. Bryden, J. Mater. Process. Technol. 139 (2003) 585.
[37] T. Miokovic, V. Schulze, O. Vohringer, D. Lohe, Mater. Sci. Eng. A 435–436 (2006) 547.
[38] S. Skvarenina, Y.C. Shin, Surf. Coat. Technol. 201 (2006) 2256.
[39] L. Orazi, A. Fortunato, G. Cuccolini, G. Tani, Appl. Surf. Sci. 256 (2010) 1913.
[40] N.S. Bailey, W. Tan, Y.C. Shin, Surf. Coat. Technol. 203 (2009) 2003.
[41] R.S. Lakhkar, Y.C. Shin, M.J.M. Krane, Mater. Sci. Eng. A 480 (2008) 209.
[42] A. Fortunato, L. Orazi, G. Tani, J. Mauf. Sci. Eng. 133 (2011) 021003-1-7.
[43] G. Tani, L. Orazi, A. Fortunato, CIRP Ann. Manuf. Technol. 57 (2008) 209.
[44] S. Safdar, L. Li, M.A. Sheikh, Z. Liu, J. Manuf. Sci. Eng. 128 (2006) 659.
[45] Michael K.H. Leung, H.C. Man, J.K. Yu, Int. J. Heat Mass Transf. 50 (2007) 4600.
[46] W. Wu, N.G. Liang, C.H. Gan, G. Yu, Surf. Coat. Technol. 200 (2006) 2686.
[47] T. Miokovic, V. Schulze, O. Vohringer, D. Lohe, Acta Mater. 55 (2007) 589.
[48] I.Y. Smurov, A.A. Uglov, A.M. Lashyn, P. Matteazzi, L. Covelli, V. Tagliaferri, Int. J. Heat Mass Transf. 34 (4/5) (1991) 961.
[49] M. Kalyon, B.S. Yilbas, Appl. Surf. Sci. 252 (2006) 2242.
[50] S.Z. Shuja, B.S. Yilbas, Shafique M.A. Khan, Int. J. Thermal Sci. 48 (2009) 1960.
[51] www.matweb.com/search/datasheet_print.aspx?matguid=c40f8cc77d5e46e1af49f7173abf34f9.
[52] W.F. Gale, T.C. Totemeir (Eds.), Smithells Metal Reference Book, 8th ed, Elsevier Butterworth-Heinmann, Oxford, 2004, p. 14.